

ORIGINAL RESEARCH

Acute Effects of Ibrutinib on Ventricular Arrhythmia in Spontaneously Hypertensive Rats



Beibei Du, MD, PhD,^{a,b,*} Praloy Chakraborty, MD,^{a,*} Mohammed Ali Azam, MBBS, PhD,^a Stéphane Massé, MASc,^a Patrick F.H. Lai, MSc,^a Ahmed Niri, BEng,^a Daoyuan Si, MD, PhD,^{a,b} Paaladinesh Thavendiranathan, MD, SM,^c Husam Abdel-Qadir, MD, PhD,^c Filio Billia, MD, PhD,^c Kumaraswamy Nanthakumar, MD^a

ABSTRACT

BACKGROUND The Bruton's Tyrosine Kinase Inhibitor ibrutinib is associated with ventricular arrhythmia (VA) and sudden death. However, the pro-arrhythmic electrophysiological dysregulation that results from ibrutinib with age and cardiovascular disease is unknown.

OBJECTIVES This study sought to investigate the acute effects of ibrutinib on left ventricular (LV) VA vulnerability, cytosolic calcium dynamics, and membrane electrophysiology in old and young spontaneous hypertensive rats (SHRs).

METHODS Langendorff-perfused hearts of young (10 to 14 weeks) and old (10 to 14 months) SHRs were treated with ibrutinib (0.1 $\mu\text{mol/l}$) or vehicle for 30 min. Simultaneously, LV epicardial action potential and cytosolic calcium transients were optically mapped following an incremental pacing protocol. Calcium and action potential dynamics parameters were analyzed. VA vulnerability was assessed by electrically inducing ventricular fibrillations (VFs) in each heart. Western blot analysis was performed on LV tissues.

RESULTS Ibrutinib treatment resulted in higher vulnerability to VF in old SHR hearts ($27.5 \pm 7.5\%$ vs. $5.7 \pm 3.7\%$; $p = 0.026$) but not in young SHR hearts ($8.0 \pm 4.9\%$ vs. 0% ; $p = 0.193$). In old SHR hearts, following ibrutinib treatment, action potential duration (APD) alternans ($p = 0.008$) and APD alternans spatial discordance ($p = 0.027$) were more prominent. Moreover, calcium transient duration 50 was longer ($p = 0.032$), calcium amplitude alternans ratio was significantly lower ($p = 0.001$), and time-to-peak of calcium amplitude was shorter ($p = 0.037$). In young SHR hearts, there were no differences in calcium and APD dynamics.

CONCLUSIONS Ibrutinib-induced VA is associated with old age in SHR. Acute dysregulation of calcium and repolarization dynamics play important roles in ibrutinib-induced VF. (J Am Coll Cardiol CardioOnc 2020;2:614–29) © 2020 The Authors. Published by Elsevier on behalf of the American College of Cardiology Foundation. This is an open access article under the CC BY-NC-ND license (<http://creativecommons.org/licenses/by-nc-nd/4.0/>).

From ^aThe Hull Family Cardiac Fibrillation Management Laboratory, Toronto General Hospital, Toronto, Ontario, Canada; ^bDepartment of Cardiology, The Third Hospital of Jilin University, Jilin Provincial Cardiovascular Research Institute, Changchun, China; and the ^cTed Rogers Program in Cardiotoxicity Prevention, Peter Munk Cardiac Center, Toronto General Hospital, University Health Network, University of Toronto, Toronto, Ontario, Canada. *Drs. Du and Chakraborty contributed equally to this work.

The authors attest they are in compliance with human studies committees and animal welfare regulations of the authors' institutions and Food and Drug Administration guidelines, including patient consent where appropriate. For more information, visit the *JACC: CardioOncology* [author instructions page](#).

Manuscript received April 24, 2020; revised manuscript received August 26, 2020, accepted August 30, 2020.

Ibrutinib is a Bruton's tyrosine kinase inhibitor used in treatments of chronic lymphocytic leukemia and other B cell-related hematologic malignancies (1,2). Unlike other cytotoxic agents, ibrutinib lacks the side effects of bone marrow suppression and mucocutaneous toxicities. Ibrutinib has cardiac toxicity that often manifests as atrial fibrillation (AF), with a reported 4-fold increased risk (3,4). However, the emerging role of ibrutinib in ventricular arrhythmias (VA) and sudden cardiac death (5,6) is poorly understood. Initial reports of VA prompted retrospective analyses of ibrutinib trials and Food and Drug Administration Adverse Event Reporting System, which documented a significant increase in VA events in patients treated with ibrutinib (7,8). Treatment with ibrutinib also has been associated with increased VA susceptibility in a mouse model (9). Mechanistic studies of ibrutinib's cardiotoxicity have been limited to cultured cardiomyocytes, where automaticity is enhanced due to both early afterdepolarizations (EADs) and delayed afterdepolarizations (DAD) with increasing late sodium current (10). Clinical evaluations of global measure of repolarization abnormalities have not demonstrated ibrutinib-induced effects on heart rate-corrected QT interval (11).

Age is considered a risk factor for developing AF in patients treated with ibrutinib (12). In the present study, we used old spontaneous hypertension rats (SHRs) to determine if VA vulnerability is increased by ibrutinib compared with younger animals. Furthermore, we investigated the underlying electrophysiological and calcium dynamics changes after an acute treatment with ibrutinib on SHR hearts perfused in a Langendorff system. We analyzed action potential duration (APD) alternans, spatially discordance of APD alternans, calcium transient duration (CaTD), calcium alternans (CA), time-to-peak on the left ventricular (LV) epicardial surface to define the acute electrophysiological alteration due to ibrutinib on VA vulnerability, repolarization, and calcium kinetics. We hypothesized that ibrutinib causes calcium cycling dysfunction and membrane repolarization dysregulation, and thus increases VA vulnerability. We also hypothesized that these abnormalities are more pronounced in hearts with advanced age and cardiomyopathy.

METHODS

EXPERIMENTAL PROTOCOL. All protocols followed the Guidelines to the Care and Use of Laboratory

Animals and were approved by the University Health Network Animal Care Committee. Young (n = 9; 10 to 14 weeks old; 220 to 330 g) and old (n = 15; 10 to 14 months; 350 to 400 g) male SHRs (Charles River Canada, Laval Quebec, Canada) were used in these experiments. Rat hearts were harvested for Langendorff perfusion and randomized into 2 groups: ibrutinib (0.1 $\mu\text{mol/l}$) and vehicle only (dimethyl sulfoxide). The 0.1 $\mu\text{mol/l}$ dose of ibrutinib was chosen based on a previous report on actions of ibrutinib by McMullen et al. (13) The calcium and voltage mappings were performed optically following 30 min of exposure to either ibrutinib or vehicle alone. Ventricular fibrillation (VF) inducibility was assessed electrically by inducing VF with high-rate, high-energy stimulation.

LANGENDORFF-PERFUSED SHR HEARTS.

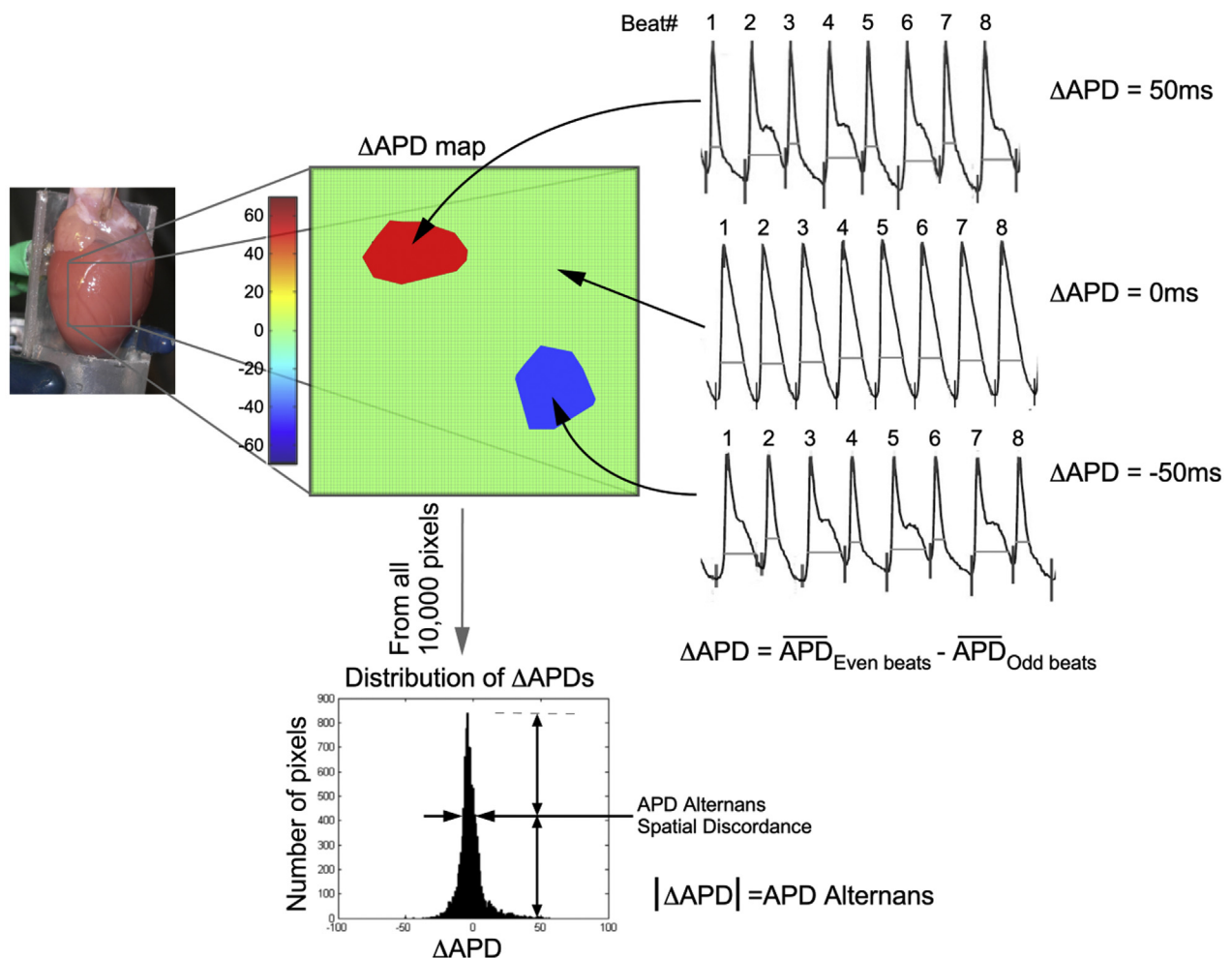
Rats were anesthetized with isoflurane (2% to 5%) and hearts were harvested through a midline thoracotomy. Each heart was then cannulated for retrograde perfusion at the Langendorff apparatus with buffer containing NaCl (130 mmol/l), NaHCO_3 (24 mmol/l), KCl (4.4 mmol/l), MgSO_4 (0.3 mmol/l), CaCl_2 (2.2 mmol/l), KH_2PO_4 (1.2 mmol/l), and glucose (6 mmol/l), equilibrated with carbogen gas (95% O_2 , 5% CO_2), maintained at 37°C and ~ 70 mm Hg.

VA VULNERABILITY. VF induction was performed by high-rate, high-energy stimulation for 10 s at 50 Hz and 12V. High-rate, high-energy stimulation was performed up to 5 times to induce VF, with 3 min of recovery after each successful VF induction. Each induced VF episode lasting for ≥ 10 s was considered a successful induction of VF and was expressed as percentage of successful VF induction in each heart.

OPTICAL MAPPING. The calcium-sensitive dye Rhod-2,AM (0.1 μmol) and the voltage-sensitive dye RH237 (0.25 μmol) were slowly infused to the perfusate solution, which also contained blebbistatin (6 μmol) to suppress cardiac motion during imaging. For optical recording of epicardial fluorescence, hearts were illuminated with a xenon light source (Moritek, Saitama, Japan) and a 530-nm green filter (Semrock, Rochester, New York) to excite dye fluorescence, and the emission light beam was bandpass filtered at 585/40 nm and then recorded at 500 frames/s using a high-speed CMOS camera (Ultima-L, Scimedica, Costa Mesa, California) with 10,000 pixels organized in a

ABBREVIATIONS AND ACRONYMS

AF	= atrial fibrillation
AMPK	= adenosine monophosphate-activated protein kinase
APD	= action potential duration
CA	= calcium alternans
CaMKII	= Ca^{2+} /calmodulin-dependent protein kinase II
CaTD	= calcium transient duration
CaT	= calcium transient
DAD	= delayed afterdepolarization
EAD	= early afterdepolarization
LV	= left ventricular
PI3K	= phosphoinositide 3-kinase
PLB	= phospholamban
SCaE	= spontaneous calcium elevation
SHR	= spontaneous hypertension rat
SR	= sarcoplasmic reticulum
VA	= ventricular arrhythmia
VF	= ventricular fibrillation

FIGURE 1 Illustrative Examples of Δ APD, APD Alternans, Δ APD Maps, and APD Alternans Spatial Discordance

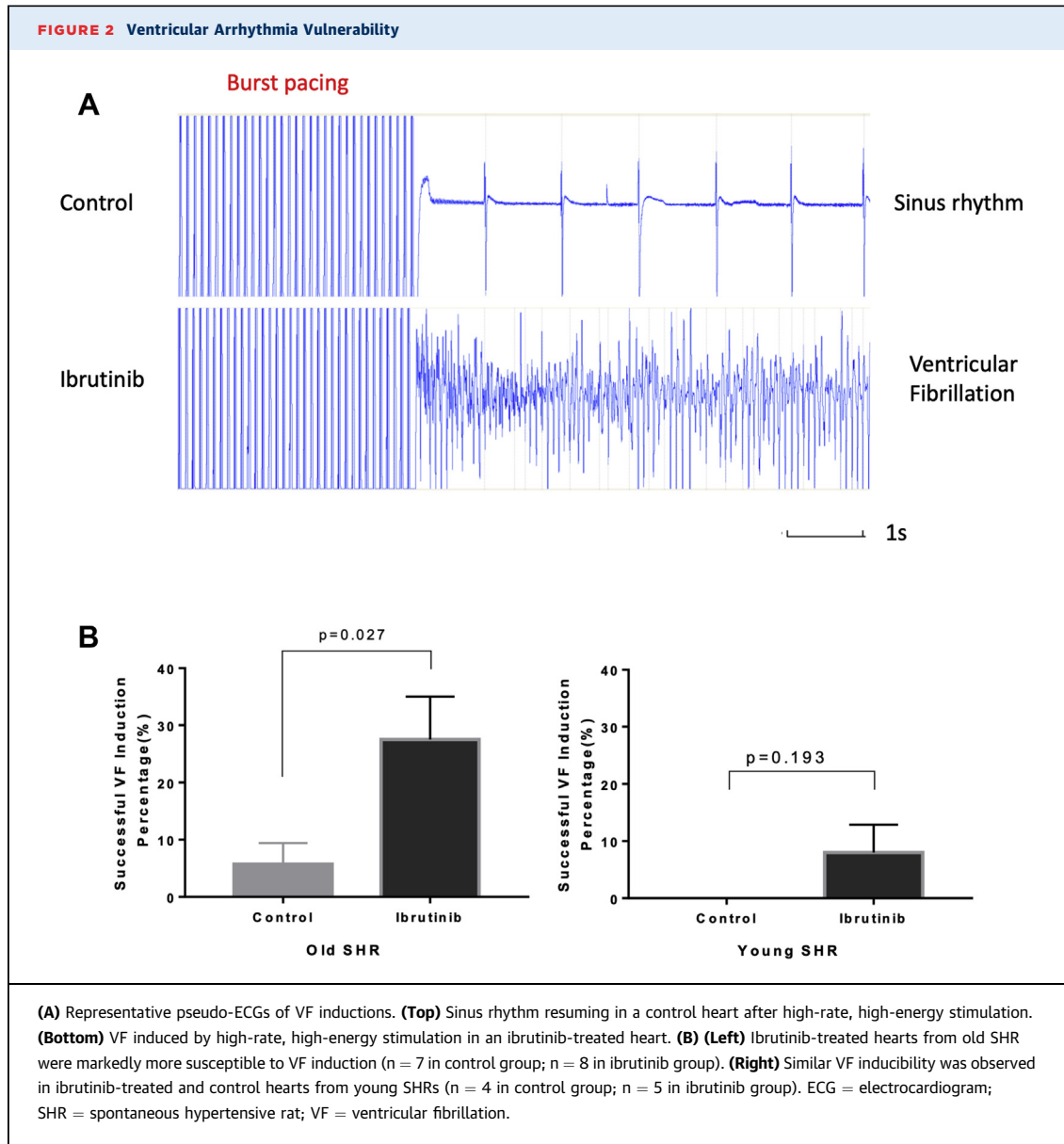
(Left) Langendorff-perfused rat heart showing the mapping area. **(Middle)** A Δ APD map showing 2 distinct zones with different Δ APDs over a Δ APD = 0 (light green) background. **(Right)** Representative action potential tracings corresponding to the 3 conditions seen on the map are depicted. **(Top)** A positive Δ APD (APD from even beats larger than odd beats); Δ APD = 0 (no alternans); negative Δ APD. **(Bottom)** A typical distribution of Δ APDs and how APD alternans spatial discordance is defined. Further information can be found in the Methods section. APD = action potential duration.

100×100 matrix on a 1-cm^2 sensor. The optical set-up was also equipped with a Leica Planapo $1.0\times$ lens at the objective, a $1.0\times$ on the condensing side, and a THT Splitter (Scimedia), which were put together to provide a spatial resolution of $100 \mu\text{m}/\text{pixel}$. A bipolar pseudo-electrogram also was recorded from a pair of electrodes mounted on a “chair” positioned behind the heart and was fed to the Ultima-L and a PowerLab input (AD Instruments, Dunedin, Otago, New Zealand) for continuous monitoring. Electrical stimulation was provided by a Grass Instruments S88X pulse

stimulator and delivered to the heart through a separate pair of electrodes.

ACTION POTENTIAL DURATION DYNAMICS. Epicardial APD dynamics were measured using incremental pacing protocol. Hearts were paced for 30 s (9.0 to 12.5 Hz) to achieve a steady state. Epicardial voltage signals were collected, and APD dynamics were assessed with parameters described as follows with a custom program written in MATLAB.

APD_{80} was chosen for repolarization duration to minimize measurement ambiguity. The mapping area

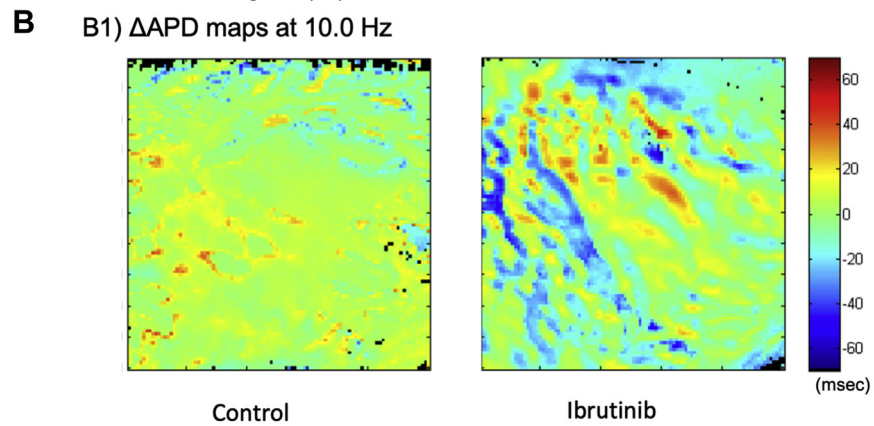
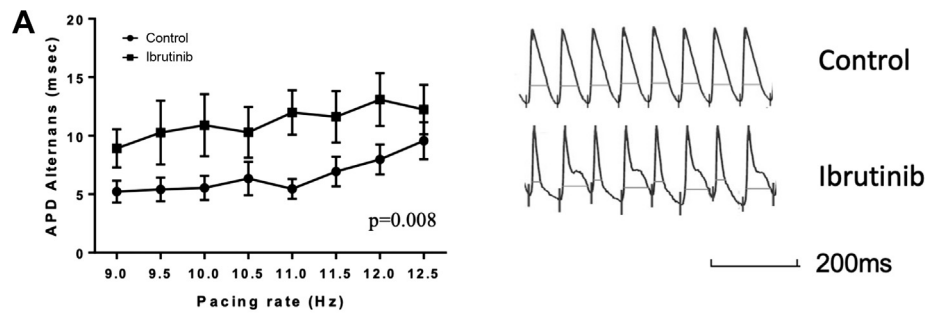


(1.0 cm²) was divided into 100 × 100 points. For each point, ΔAPD and APD alternans were calculated using the formula: $\Delta APD = \frac{\sum(APD_{Even\ beats})}{n_e} - \frac{\sum(APD_{Odds\ beats})}{n_o}$ where $\frac{\sum(APD_{Even\ beats})}{n_e}$ and $\frac{\sum(APD_{Odds\ beats})}{n_o}$ represented the average APD from even and odd beats, respectively, in a recording. We defined APD alternans as the absolute value of ΔAPD. Additional definitions are as follows. APD alternans at a specific pacing rate is the mean value of all 100 × 100 points in the map. ΔAPD map is a representation

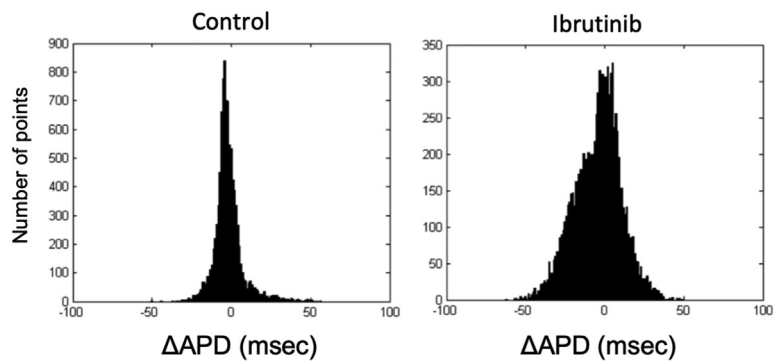
of ΔAPD measured at each point. Values of ΔAPD are shown in a scale varying from positive ΔAPD (shown in red) to negative ΔAPD (blue). Points with no alternans (ΔAPD = 0) appear in green. Missing or out-of-range data are represented with black points. **Figure 1** shows an example of how ΔAPD maps are generated.

Distribution of ΔAPD was presented as histogram summarizing the 10,000 points (100 × 100) being analyzed (**Figure 1**). The x-axis indicates the different

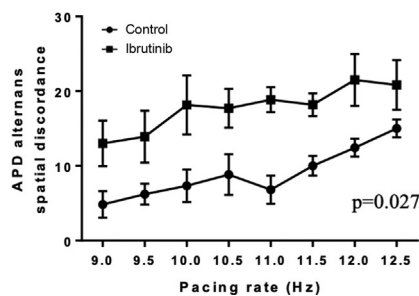
FIGURE 3 APD Alternans and APD Alternans Spatial Discordance in Old SHR



B2) Distributions of Δ APD at 10.0 Hz



B3) APD Alternans Spatial Discordance



Δ APD values; y-axis indicates the number of points of a certain Δ APD value.

APD alternans spatial discordance at a certain pacing rate was quantified as the width of the half-peak value of the Δ APD distribution histogram. Discordance value is 0 when all the points on the map have same Δ APD value.

APD₅₀ and APD₈₀ measurements represent the durations from time 0 to 50% and 80% repolarization of APD were measured using MATLAB code.

In calcium mapping, calcium transient signals (CaTs) were collected simultaneously with voltage signals. Following the 30 s (9.0 to 12.5 Hz) pacing, the perfused heart was stimulated according to a “pace & pause” protocol as we reported previously (14), and calcium signals between the last 2 s of pacing and the first 2 s of spontaneous rhythm were collected. Three representative pixels from the mapped area were selected, decoded, and quantified with a custom MATLAB program written for assessment of the following parameters of CaTs.

CaTs amplitude alternans was defined as the average of amplitude of Ca²⁺ signal of even beats compared with that of odd beats during beat-to-beat pacing, and is represented as a ratio (smallest Ca²⁺ signals)/(largest Ca²⁺ signals), where largest and smallest Ca²⁺ signals are each derived from either odd or even beats (15).

Time-to-peak of CaTs upstrokes was calculated as the time duration for fluorescence to change from 0% to 100% of maximum.

CaTD₅₀ and CaTD₈₀ represent the duration from depolarization to 50% or 80% of repolarization of CaTs. Baseline for each beat is defined as the fluorescence level immediately before depolarization.

Spontaneous calcium elevation (SCaE) is the calcium signal elevation between the last pacing beat and the first spontaneous beat calculated as reported in our previous article (14).

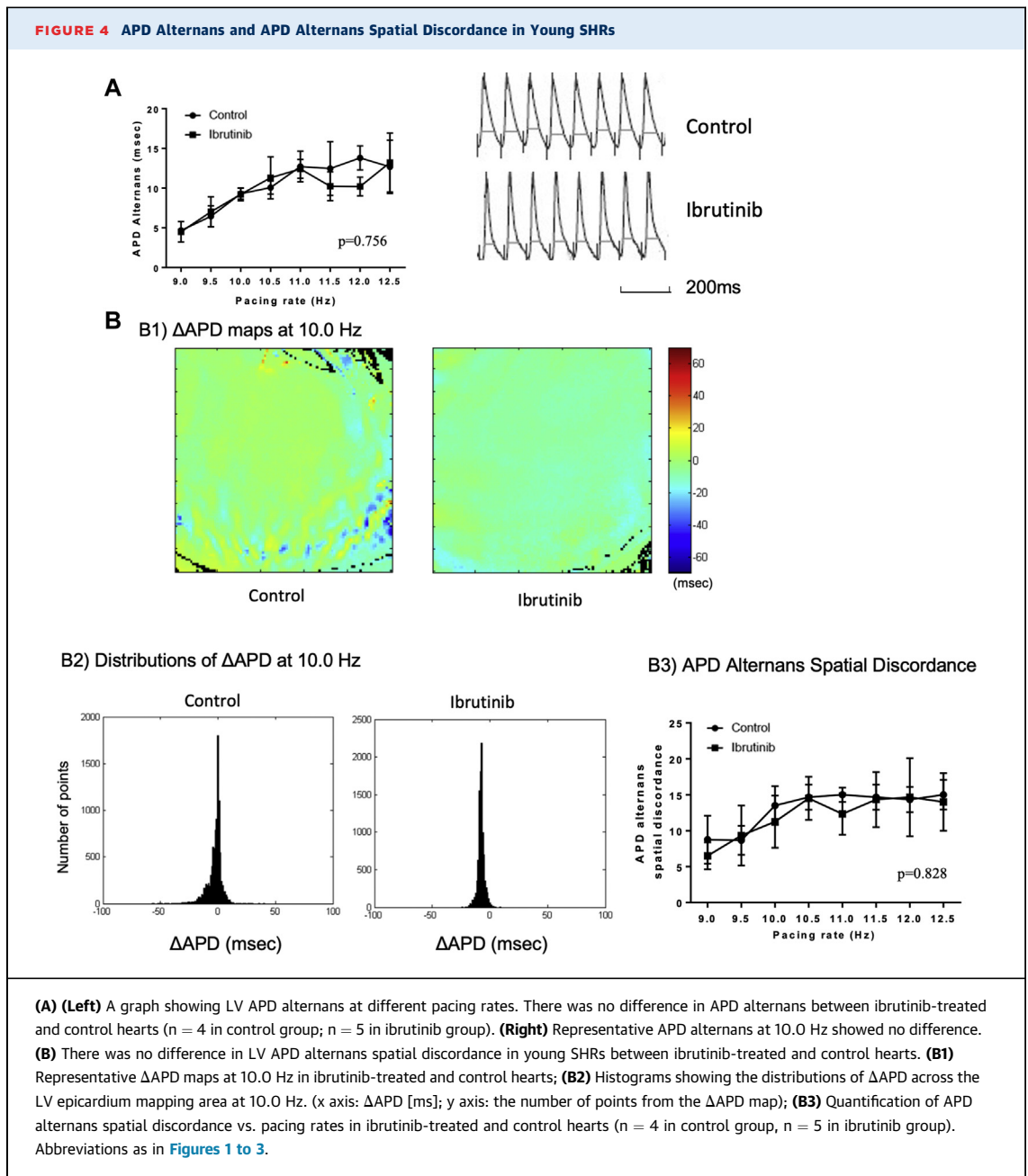
WESTERN BLOT ANALYSIS. Western blot analysis for the phosphorylated or total abundance of phosphoinositide 3-kinase (PI3K) 110 α (Cell Signaling, Danvers,

Massachusetts; 1:2,000 dilution) and Akt (both total and phosphorylated Akt antibodies from Sigma; 1:3,000), phospholamban (PLB) (total PLB, PLB Ser16, PLB Thr17 antibodies from Badrilla, Leeds, West Yorkshire, United Kingdom; 1:5,000), SERCA2a (Badrilla; 1:5,000), Ca_v1.2 (total Ca_v1.2 antibody from Sigma and phosphorylated Ca_v1.2 antibody from Badrilla; both 1:1,000) and Ca²⁺/calmodulin-dependent protein kinase II (CaMKII; Badrilla, 1:3,000), adenosine monophosphate-activated protein kinase (AMPK; both total and phosphorylated AMPK from Cell Signaling; 1:3,000), and NCX (biorbyt, Cambridge, Cambridgeshire, United Kingdom, 1:3,000) proteins were performed. In brief, frozen LV tissue was mechanically homogenized in a lysis buffer containing 30 mmol/l KH₂PO₄, 0.5mmol/l dithiothreitol, 0.3 mol/l sucrose, and a cocktail of phosphatase and protease inhibitors (Roche, Laval, Quebec, Canada). Solubilized proteins were resolved using sodium dodecyl sulphate-polyacrylamide gel electrophoresis. Separated proteins were transferred onto polyvinylidene difluoride membranes. The membranes were incubated with specific antibodies followed by incubation with horseradish peroxidase-conjugated secondary antibodies. An enhanced chemiluminescence kit was used to visualize proteins. Protein band signals were digitally recorded using the Microchemi4.2 imaging system (FroggaBio, Concord, Ontario, Canada) for analysis with the National Institutes of Health ImageJ software. Western blot analysis of RyR2 (total RyR2 antibody from Thermo Scientific, Waltham, Massachusetts, phosphorylated RyR2 antibody from Badrilla; both 1:3,000) was performed according to a previously published protocol (15).

STATISTICAL ANALYSIS. Data are expressed as mean \pm SEM. The unpaired *t* test was used to compare the incidence of VF. Two-way repeated measure analysis of variance was performed to compare continuous variables in the analysis of CaTD₅₀, CaTD₈₀, CaTD₅₀/CaTD₈₀ ratio, CaTs amplitude alternans index, time-to-peak, SCaE, APD alternans, and spatial

FIGURE 3 Continued

(A) (Left) A graph showing LV APD alternans at different pacing rates. Ibrutinib increased APD alternans in old SHR hearts compared with controls (n = 7 in each group). **(Right)** Representative tracings with increased APD alternans from an ibrutinib-treated heart and less APD alternans from a control heart at the pacing rate of 10.0 Hz. **(B)** Ibrutinib increased APD alternans spatial discordance in old SHR. **(B1)** Representative Δ APD maps at 10.0 Hz in ibrutinib-treated and control hearts. **(B2)** Histograms showing the distributions of Δ APD across the LV epicardium mapping area when stimulating the heart at 10.0 Hz (x axis: Δ APD [ms]; y axis: the number of points from the Δ APD map). **(B3)** Quantification of APD alternans spatial discordance vs. pacing rates in ibrutinib-treated and control hearts (n = 7 in each group). LV = left ventricular; other abbreviations as in Figures 1 and 2.

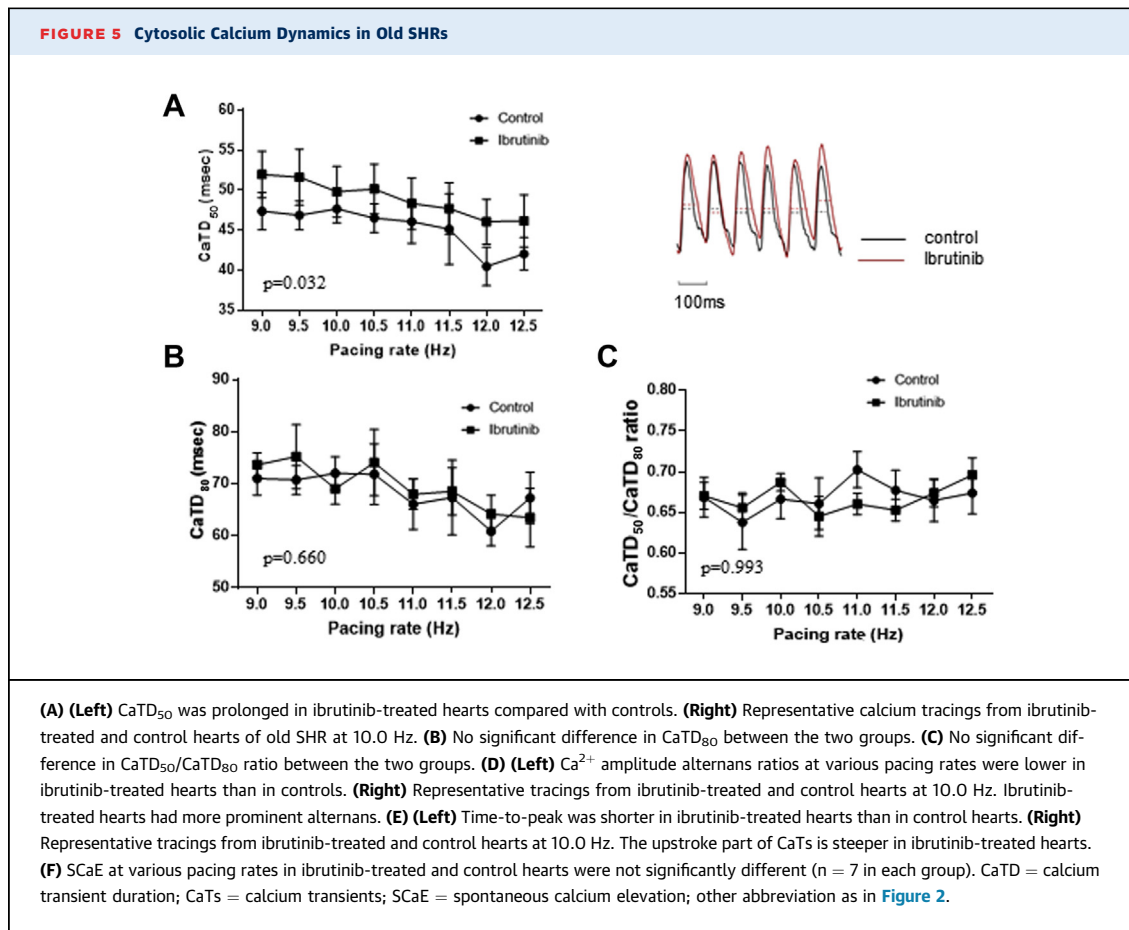


discordance of APD alternans at different pacing rates (9.0 to 12.5 Hz). To give the sense of the effect size in the results, the representative result at 10 Hz and overall p value of 2-way analysis of variance are shown. Unpaired *t* tests were performed to compare differences in protein band intensity in Western blots. A p value <0.05 was considered as statistically significant. Data analysis was performed using GraphPad Prism 7.00 and SPSS 22.0.

RESULTS

EFFECT OF IBRUTINIB ON VA VULNERABILITY.

Hearts were subjected to rapid electrical pacing to assess the inducibility of arrhythmias as described in Methods. In old SHR hearts, VF was more readily induced in the presence of ibrutinib ($n = 8$), yielding a higher rate of VF induction at $27.5 \pm 7.5\%$ (vs. $5.7 \pm 3.7\%$ in controls; $n = 7$; $p = 0.027$) ([Figure 2](#)). This



Continued on the next page

significantly higher VA vulnerability was not observed in young SHR hearts (n = 5) under the same ibrutinib treatment (successful VF induction rate 8.0 ± 4.9% vs. 0 ± 0% in controls; n = 4; p = 0.193). These data suggest that a higher incidence of ibrutinib-induced VA is associated with aging.

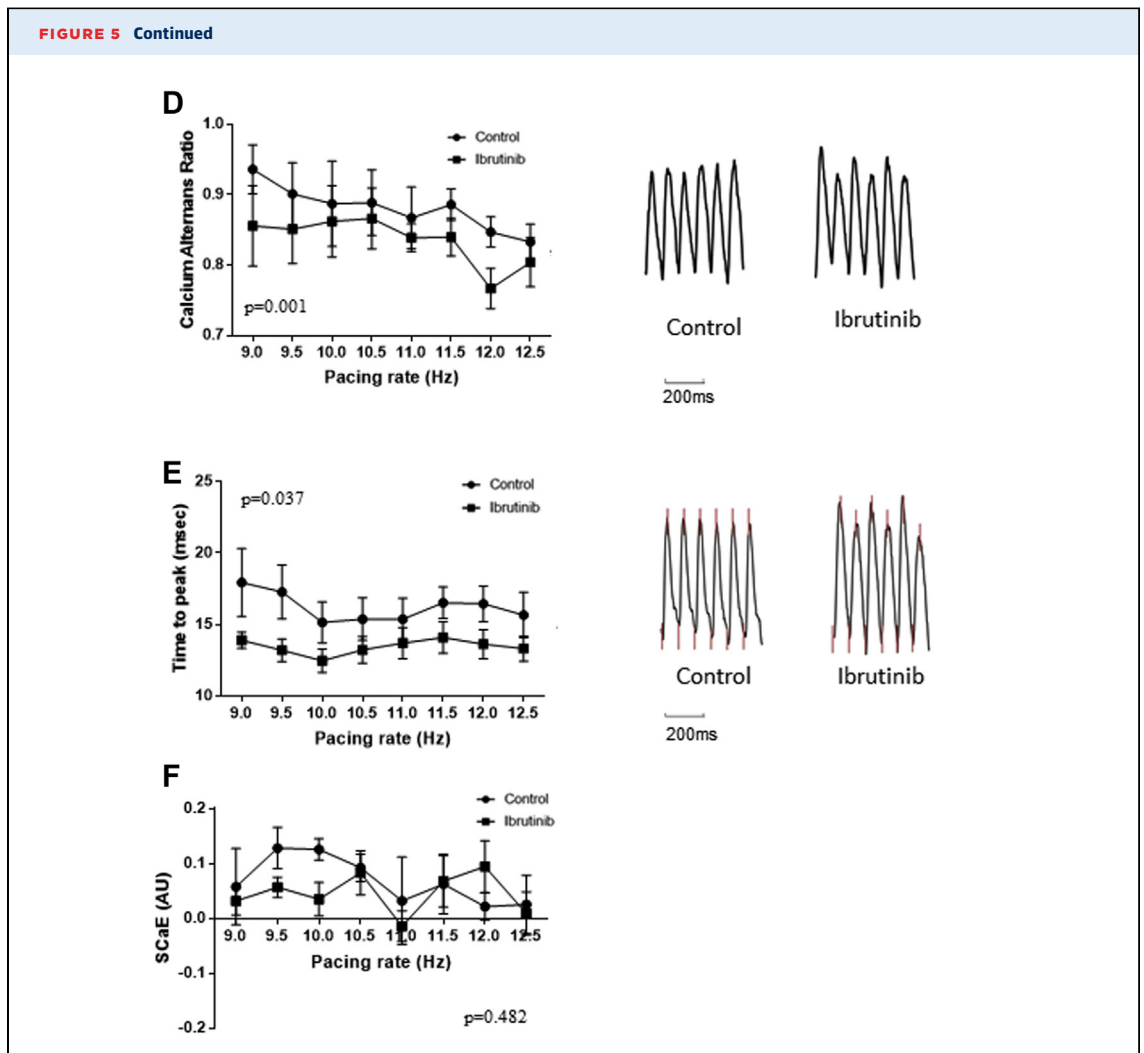
EFFECT OF IBRUTINIB ON APD ALTERNANS AND APD ALTERNANS SPATIAL DISCORDANCE. APD alternans was assessed at various pacing rates and the results are shown in [Figures 3A](#) and [4A](#). In ibrutinib-treated hearts, APD alternans was more prominent in old SHRs compared with control (10.9 ± 2.6 ms vs. 5.5 ± 1.0 ms at 10 Hz; p = 0.008) ([Figure 3A](#)). In young SHRs, no difference in APD alternans was observed (p = 0.756) ([Figure 4A](#)).

LV APD alternans spatial discordance from old and young SHRs are shown in [Figures 3B](#) and [4B](#). In ibrutinib-treated hearts, APD alternans spatial discordance was more prominent in old SHRs

compared with controls (18.2 ± 4.0 ms vs. 7.3 ± 2.2 ms at 10.0 Hz; p = 0.027) ([Figure 3B](#)). In contrast, in young SHRs, no difference in APD alternans spatial discordance was found (p = 0.828) ([Figure 4B](#)).

EFFECT OF IBRUTINIB ON APD₅₀ AND APD₈₀. There was no significant difference in APD₅₀ (p = 0.232) and APD₈₀ (p = 0.571) in old and young SHRs (APD₅₀ p = 0.925 APD₈₀ p = 0.734) between ibrutinib-treated and control hearts ([Supplemental Figure 1](#)).

EFFECTS OF IBRUTINIB ON CALCIUM DYNAMICS. In ibrutinib-treated groups, there were longer CaTD₅₀ (49.8 ± 3.27 ms vs. 47.7 ± 1.7 ms at 10.0 Hz; p = 0.032), lower CaTs amplitude alternans ratios (0.86 ± 0.05 vs. 0.89 ± 0.06 at 10.0 Hz; p = 0.001), and shorter time-to-peak (12.5 ± 0.8 ms vs. 15.2 ± 1.4 ms at 10.0 Hz; p = 0.037) in old SHRs, whereas no difference was observed in CaTD₈₀ (69 ± 3.0 ms vs. 72.0 ± 3.2 ms at 10.0 Hz; p = 0.660), CaTD₅₀/CaTD₈₀ ratio (0.69 ± 0.01 vs. 0.67 ± 0.02 at 10.0 Hz; p = 0.993), and SCaE (0.04 ±



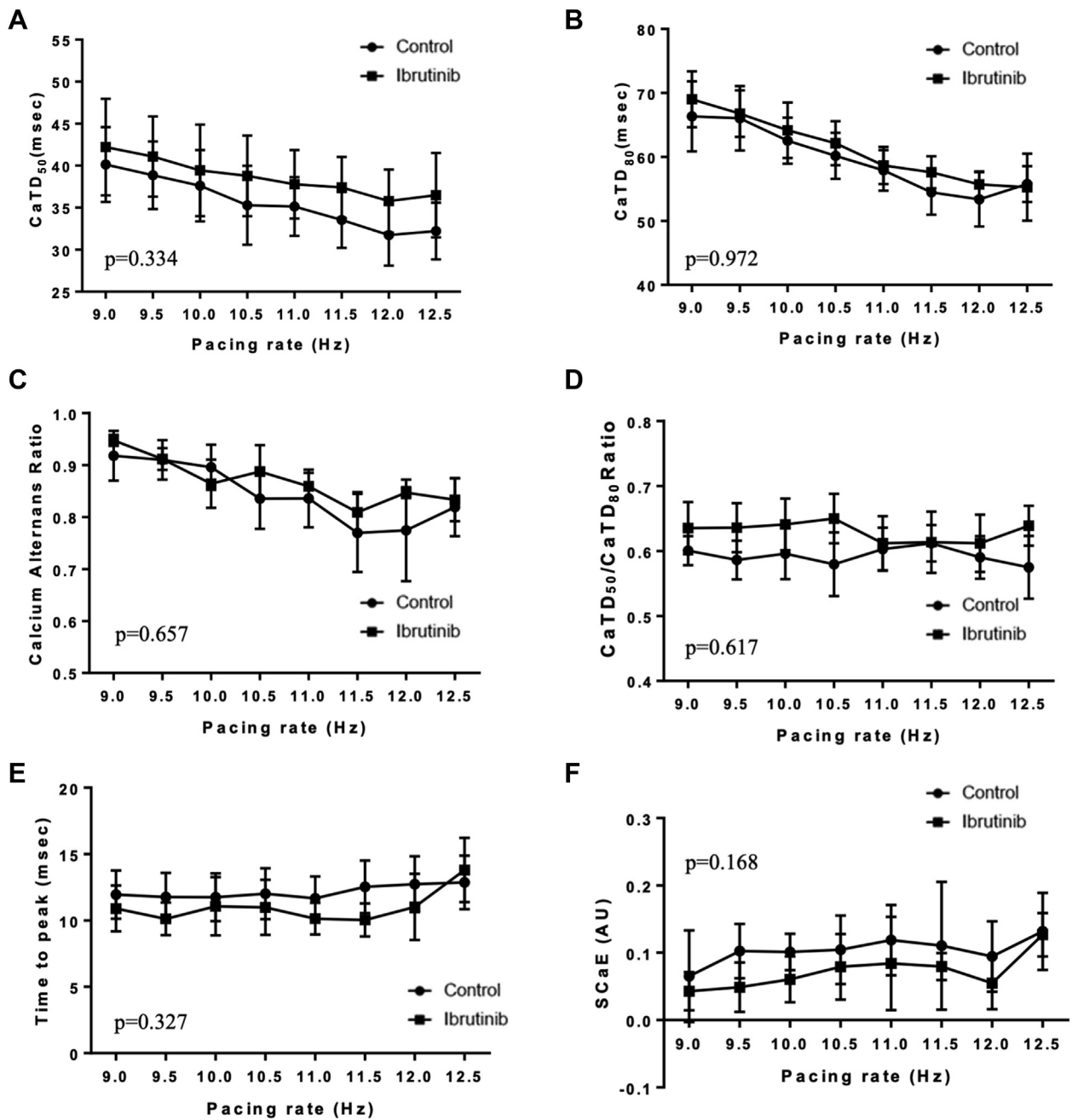
0.03 vs. 0.12 ± 0.02 at 10.0 Hz; $p = 0.482$) (Figure 5). In young SHRs, there was no difference in CaTD_{50} (39.4 ± 5.5 ms vs. 37.6 ± 4.3 ms at 10.0 Hz; $p = 0.334$), CaTD_{80} (64.2 ± 4.4 ms vs. 62.6 ± 3.6 ms at 10.0 Hz; $p = 0.972$), $\text{CaTD}_{50}/\text{CaTD}_{80}$ ratio (0.64 ± 0.04 vs. 0.60 ± 0.04 at 10.0 Hz; $p = 0.617$), CaTs amplitude alternans (0.86 ± 0.05 vs. 0.90 ± 0.04 at 10.0 Hz; $p = 0.657$), time-to-peak (11.1 ± 2.2 ms vs. 11.8 ± 1.8 ms at 10.0 Hz; $p = 0.327$), and SCaE (0.06 ± 0.03 ms vs. 0.10 ± 0.03 ms at 10.0 Hz; $p = 0.168$) between ibrutinib-treated and control groups (Figure 6).

EFFECTS OF IBRUTINIB ON CALCIUM HANDLING PROTEINS. To determine the pathway of ibrutinib-induced cardiac arrhythmias and calcium dysregulation, we performed Western blot analysis for phosphorylation and expression of PLB, SERCA2a, NCX,

CaMKII, $\text{Ca}_v1.2$, and RyR2 in LV tissues. We found no difference in the phosphorylation of PLB at Ser16 (1.00 ± 0.37 vs. 1.02 ± 0.56 ; $p = 0.160$), Thr17 (1.00 ± 0.08 vs. 0.83 ± 0.09 ; $p = 0.977$), and SERCA2a (1.0 ± 0.04 vs. 1.02 ± 0.02 ; $p = 0.670$) between controls and ibrutinib-treated groups, respectively, in old SHRs (Figures 7A to 7C). We also found no difference in RyR2 phosphorylation at Ser2808 and Ser2814 (1.00 ± 0.14 vs. 0.89 ± 0.09 ; $p = 0.506$; and 1.00 ± 0.31 vs. 1.03 ± 0.47 ; $p = 0.965$, respectively) between the 2 groups of old SHRs (Figures 7D and 7E). No difference in expression of NCX and phosphorylation of CaMKII at Thr286 and $\text{Ca}_v1.2$ at Ser1928 between the 2 groups of old SHRs were found (Supplemental Figure 2).

EFFECTS OF IBRUTINIB ON PI3K-AKT AND AMPK PATHWAYS. Western blotting also was performed to

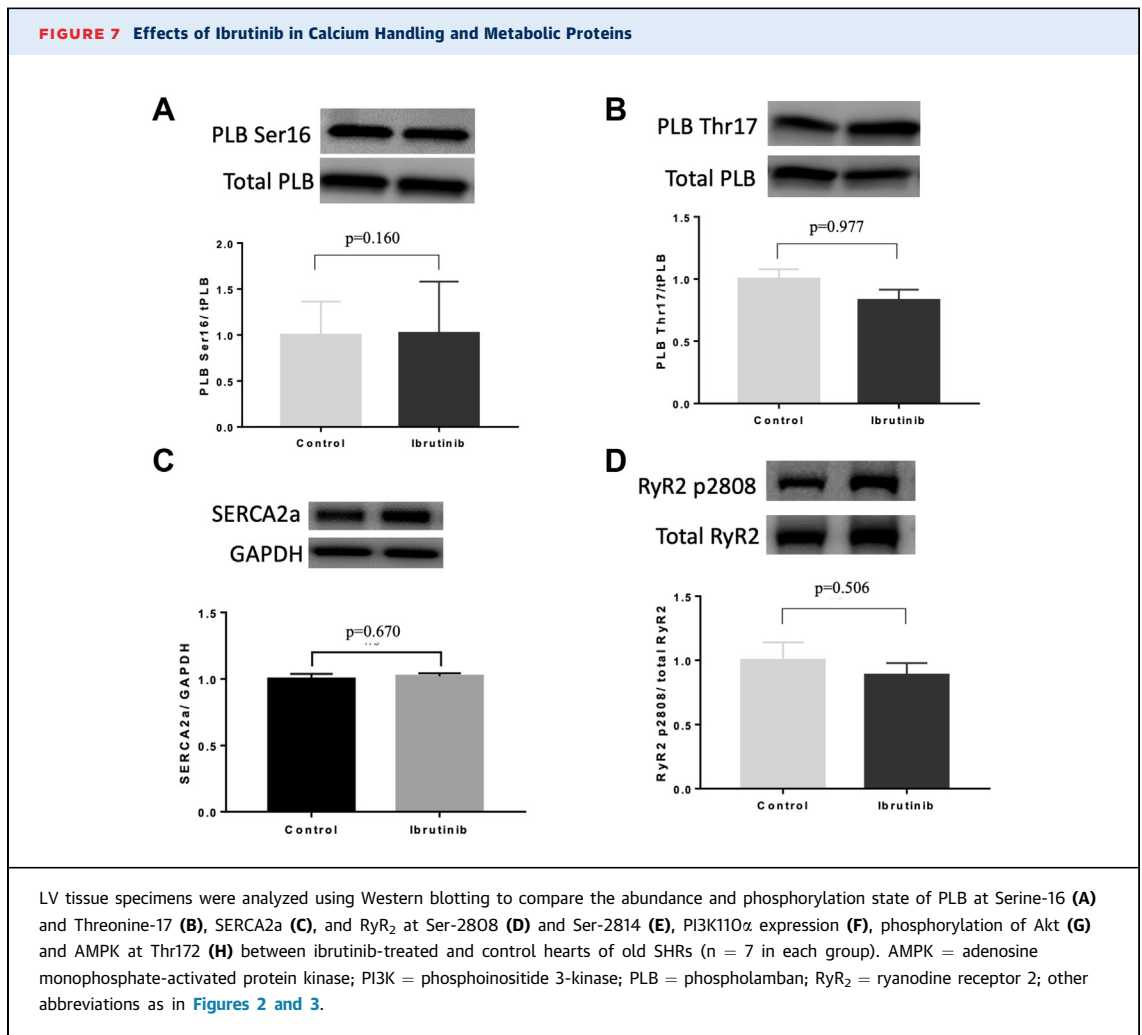
FIGURE 6 Cytosolic Calcium Dynamics in Young SHR



There were no differences in CaTD₅₀ (A), CaTD₈₀ (B), CaTD₅₀/CaTD₈₀ ratio (C), calcium alternans ratio (D), time-to-peak (E), and spontaneous calcium elevation (F) in ibrutinib-treated and control hearts from young SHR (n = 4 in control group, n = 5 in ibrutinib group). Abbreviations as in Figures 2 and 5.

assess the effects of ibrutinib on the expression of PI3K110 α , as well as the phosphorylation state of AKT and AMPK. No differences in PI3K110 α expression (1.00 \pm 0.04 vs. 1.01 \pm 0.06; p = 0.905) (Figure 7F),

phosphorylation levels of Akt (1.00 \pm 0.07 vs. 1.16 \pm 0.14; p = 0.327) (Figure 7G), and AMPK (1.00 \pm 0.04 vs. 1.01 \pm 0.06; p = 0.905) (Figure 7H) were found between the 2 groups of old SHR.



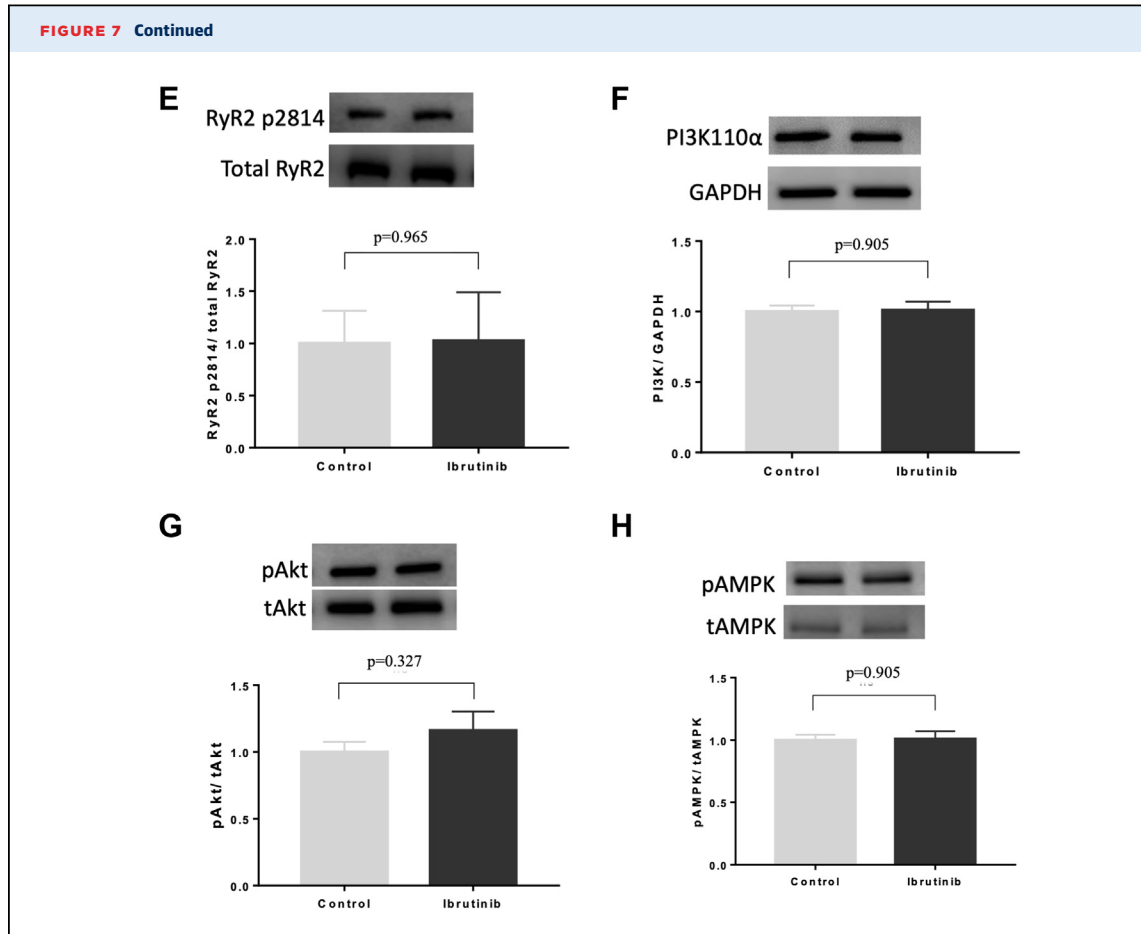
Continued on the next page

DISCUSSION

Our study demonstrated that acute treatment with ibrutinib resulted in higher vulnerability to VF in old but not in young SHR hearts. Our optical mapping demonstrated that this higher vulnerability was associated with higher rate of calcium release from the sarcoplasmic reticulum (SR), impaired cytosolic calcium clearance during diastole along with arrhythmogenic alteration of repolarization dynamics of ventricular myocardium (Central Illustration). In the literature, age has been described as a risk factor for ibrutinib-induced AF, and this study provides the unique electrophysiological basis for this vulnerability in the ventricles.

IBRUTINIB AND ACTION POTENTIAL DYNAMICS. To the best of our knowledge, the role of ibrutinib in resultant electrophysiological substrate for VA has

not been reported. Our study has demonstrated that acute treatment with ibrutinib was associated with more prominent spatially discordant APD alternans in old SHR but not in young SHR. Repolarization is represented by APD and dynamic variability of APD with pacing (APD alternans) is a recognized risk factor for arrhythmias and sudden cardiac death (16). Repolarization heterogeneity forms the milieu for functional reentry. Microvolt T-wave alternans, an electrocardiogram manifestation of cellular APD alternans, is also considered a clinically useful tool to predict risk of VAs and sudden cardiac death (17,18). Any form of APD alternans, concordant or discordant, is arrhythmogenic (19). However, spatially discordant APD alternans is considered more arrhythmogenic (16,20). The presence of discordant alternans indicates conversion of the “physiological repolarization heterogeneity” to a “pathological heterogeneity” (16). A spatial and temporal dispersion of



repolarization, by altering the refractory period, can lead to conduction block, a prerequisite for functional re-entry of VF (21).

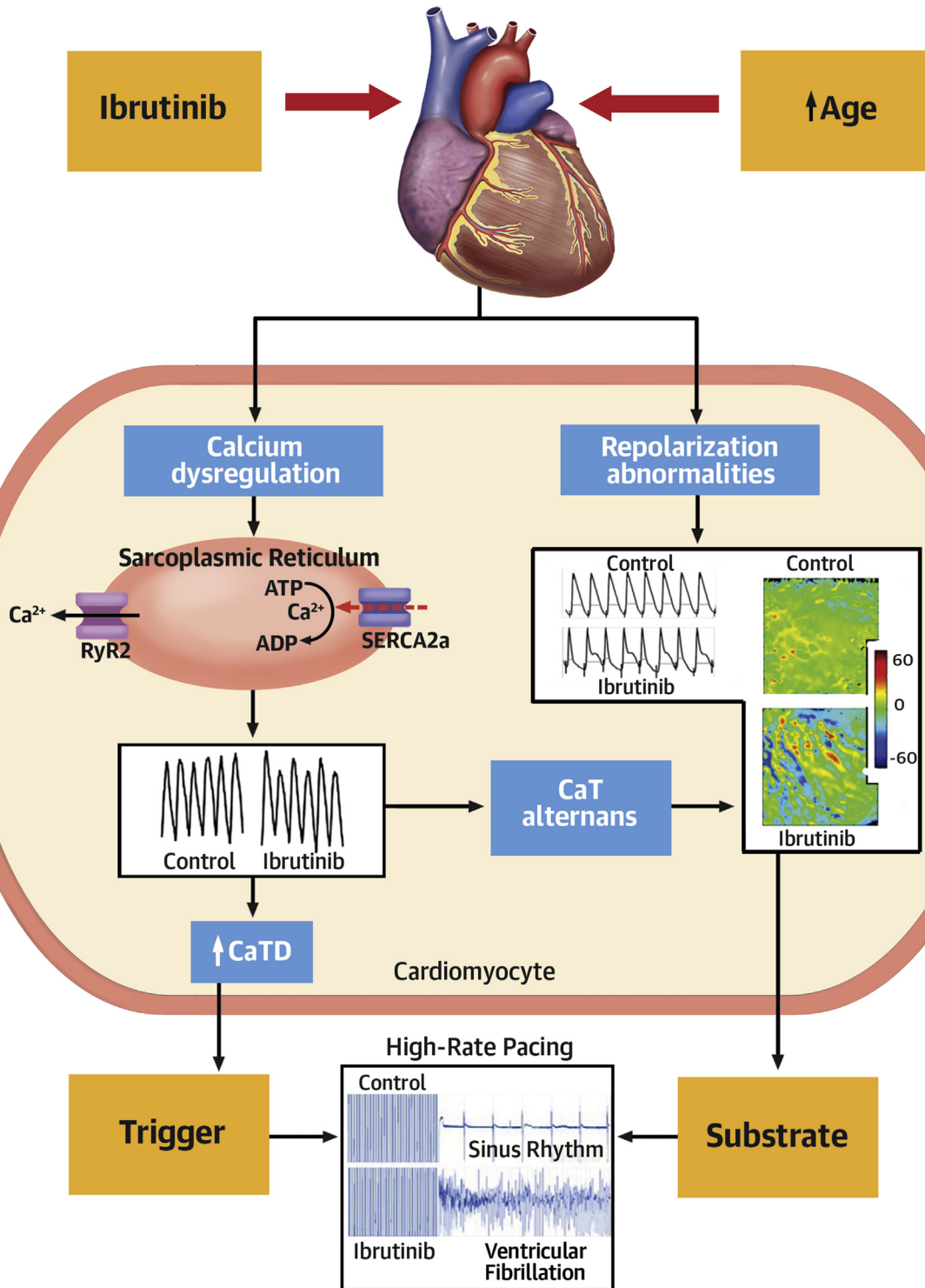
IBRUTINIB AND CALCIUM DYNAMICS. Treatment with ibrutinib was associated with shorter time-to-peak and longer CaTD₅₀ in old SHR hearts but not in young SHR, compatible with abnormalities observed in both upstroke and extrusion phase of CaTs (22). A shorter time-to-peak indicates increased rate of calcium release from SR due to abnormal RyR2 activity (22), whereas longer CaTD₅₀ represents reduced SERCA2a-mediated uptake during diastole (22,23). Initial calcium influx into the cytoplasm via the sarcolemmal Ca²⁺ channel during systole is about 6% of the SR Ca²⁺ content and 68% of influxed cytosolic Ca²⁺ efflux through Na/Ca²⁺ exchanger (24). Cytosolic calcium overload during diastole is associated with EADs or DADs, thereby initiating the trigger for arrhythmia. Ibrutinib is reported to be associated with impaired diastolic calcium clearance and generation of DADs in atrial but not ventricular cardiomyocytes (25). A quick calcium release, as

indicated by shorter time-to-peak, is reportedly associated with generation of DADs (26).

CaTs amplitude alternans is associated with VA and atrial arrhythmias (27,28). Also, CaTs amplitude is reported to control membrane electrophysiology by electrogenic feedback on repolarization (28). Dysregulated calcium dynamics in our study is suggestive of abnormalities in both calcium release and uptake mechanism of SR. Impairment of sarcoplasmic calcium handling is associated with CaTs amplitude alternans, thereby triggering APD alternans (29). We measured epicardial surface calcium and APD dynamics; transmural calcium and APD dynamics, which might contribute to dispersion and arrhythmogenesis, cannot be assessed.

IBRUTINIB-INDUCED VA AND MECHANISTIC INSIGHT. To explore the mechanism by which ibrutinib's arrhythmogenic effects are mediated, we analyzed LV expression and phosphorylation of RyR2, SERCA2a, PLB, NCX, CaMKII, Ca_v1.2, AMPK, PI3K110α, and AKT using Western blotting. Despite demonstrable changes in calcium handling, we did not

CENTRAL ILLUSTRATION Ibrutinib Increases VA Vulnerability in Old SHRs



observe any change in phosphorylation and expression status of RyR2, PLB, SERCA2a, NCX, Ca_v1.2, and CaMKII with acute exposure to ibrutinib. However, it has been previously demonstrated that chronic treatment with ibrutinib is associated with enhanced expression of CaMKII and phosphorylation of RyR2-Ser2814 and PLB-Thr17 (25). In our study, we were unable to demonstrate increased phosphorylation of RyR2; other mechanisms that may explain the abnormal calcium release kinetics include increased sensitivity of RyR2 to calcium with abnormal sarcoplasmic calcium release, which can occur in the absence of RyR2 phosphorylation (30) by enhancing oxidation (31), nitrosylation (32), and unzipping of RyR2 (33). A change in expression of proteins is not expected with acute treatment. Although phosphorylation is considered a major mechanism for functional modifications of calcium regulatory proteins, the absence of change in phosphorylation of RyR2, PLB, CaMKII, Ca_v1.2, AMPK, PI3K, and AKT in our Western blots suggests that alternate pathways of functional modifications of cellular calcium regulatory proteins may be mediators of the ibrutinib-induced changes in arrhythmia susceptibility and calcium dynamics observed in our study. Bruton's tyrosine kinase inhibition by ibrutinib is associated with mitochondrial dysfunction, altered mitochondrial redox state, and cellular energy depletion (34). Metabolic stress is associated with abnormal calcium release and impaired diastolic clearance due to effects of glycolytic intermediates on RyR2 and diminution of SERCA2a activity due to lack of adenosine triphosphate (35,36). Aberrant redox signaling is also associated with abnormal calcium transient. Besides phosphorylation, multiple post-translational modifications, such as oxidation and sulfoxidation, of calcium regulatory proteins are also described to be associated with reduced mitochondrial redox state (37).

AMPK, a cellular stress sensing molecule, is phosphorylated and activated in leukemic cells upon inhibition of mitochondrial ATP synthesis by

oligomycin as well as during ibrutinib-induced metabolic stress (34). Increased AMPK phosphorylation is also observed in ibrutinib-resistant leukemic cells (34). In contrast, AMPK inhibition is found to increase the sensitivity of leukemic cells to the cytotoxic effect of ibrutinib (34). In cardiomyocytes, ibrutinib has been reported to reduce the activity of PI3K-Akt (13). AMPK is a key upstream kinase responsible for Akt activation under metabolic stresses (38). In our study, ibrutinib treatment failed to alter the expression and phosphorylation of AMPK in old SHR hearts. Less AMPK reserve has been reported in old age and hypertension (39). The old SHRs may already have a small AMPK reserve at a level too low to be further reduced, thus AMPK expression or phosphorylation may be unaltered in our Western blots. It is also conceivable that changes in AMPK involve translocation between subcellular compartments, as observed previously in liver cells (40), and such changes would be difficult to assess in our experimental design. During metabolic stress, AMPK is involved in favorable modifications of cytosolic calcium dynamics and membrane electrophysiology (39). Altogether, our findings do not exclude the involvement of AMPK. We also acknowledge that the species might contribute to differences in AMPK activation. We were unable to demonstrate any change in the expression and phosphorylation of VDCC, NCX, and CaMKII in our acute treatment model. Consequently, increased calcium-induced calcium release by altering VDCC, NCX, and CaMKII could be a possible mechanism of ibrutinib-induced VA that needs to be explored following chronic treatment. There was no adverse effect in young SHRs at age 10 to 14 weeks following acute ibrutinib treatment, suggesting that aging plays an important role in the pathogenesis of ibrutinib-induced VA. Many factors related to aging, such as hypertrophy, fibrosis, and endocrine, renal, and neuronal changes (41,42), may contribute to the increased susceptibility to ibrutinib-induced cardiotoxicity in older SHRs, which needs to be explored.

CENTRAL ILLUSTRATION Continued

In old SHRs, acute exposure of ibrutinib is associated with cytosolic Ca²⁺ dysregulation and aberration in membrane electrophysiology. The components of Ca²⁺ dysregulation include shortening TTP, prolongation of CaTD₅₀, and Ca²⁺ transient alternans. The alteration in membrane electrophysiology is characterized by spatially discordant APD alternans. Shortening of TTP and prolongation of CaTD₅₀ led to the generation of afterdepolarization (early or late), which triggers VA. Calcium transient alternans is also linked to membrane repolarization alternans. Repolarization heterogeneity, as indicated by discordant APD alternans, constitutes the substrate for VA. A combination of triggers and the vulnerable substrate is translated into an increased propensity to VF following ibrutinib treatment. APD = action potential duration; C = control, CaT = calcium transient; CaTD₅₀ = calcium transient duration 50; SERCA2a = sarco/endoplasmic reticulum Ca²⁺-ATPase; SHR = spontaneous hypertensive rat; SR = sarcoplasmic reticulum; RyR2 = Ryanodine Receptor 2; TTP = time to peak; VA = ventricular arrhythmia; VF = ventricular fibrillation.

STUDY LIMITATIONS. The findings of this study provide interesting insights although we have evaluated only the acute effects. Chronic drug administration and myopathic changes need additional studies with in vivo characterization to evaluate mechanisms that lead to these electrophysiological changes. Those studies will be crucial for possible preventive or effective treatment strategies to be developed. In our experimental model, we did not use albumin to balance the oncotic pressure, which may cause edema over time; to avoid problems associated with tissue edema, we ran our Langendorff experiments quickly and efficiently. We also acknowledge that the differences found in our study were not compared with normal, healthy rats; the SHR are hypertensive and not perfectly healthy.

CONCLUSIONS

Acute administration of ibrutinib in SHRs leads to higher VA vulnerability, importantly and differentially in older animals but not in young SHRs, suggesting that aging contributes to ibrutinib-induced VA. The development of spatially discordant APD alternans and impaired calcium dynamics form the substrates for ventricular arrhythmogenesis. The molecular mechanisms mediating these cardiotoxic effects of ibrutinib remain to be elucidated.

ACKNOWLEDGMENT The authors would like to express their gratitude to Mr. Arulalan Veluppillai for his assistance in the preparation of various figures in this manuscript.

AUTHOR DISCLOSURES

This study was supported by the generous contributions of the Crispino family and the Hang Tough Initiative. Dr. Nanthakumar is a consultant for Servier, Biosense Webster, Abbott, and BlueRock Therapeutics. Dr. Nanthakumar is a recipient of a Mid-Career

Investigator Award from the Heart & Stroke Foundation of Ontario. Dr. Thavendiranathan (147814) is supported by the Canadian Institutes of Health Research New Investigator Award and a Canada Research Chair in Cardio-oncology. All other authors have reported that they have no relationships relevant to the contents of this paper to disclose.

ADDRESS FOR CORRESPONDENCE: Dr. Kumaraswamy Nanthakumar, The Hull Family Cardiac Fibrillation Management Laboratory, Division of Cardiology, Toronto General Hospital, University Health Network, GW3-526, 150 Gerrard Street West, Toronto, Ontario M5G 2C4, Canada. E-mail: kumar.nanthakumar@uhn.ca. Twitter: [@BeibeiDu5](https://twitter.com/BeibeiDu5).

PERSPECTIVES

COMPETENCY IN MEDICAL KNOWLEDGE: The use of ibrutinib has significantly improved cancer outcomes in patients with various hematologic malignancies. However, ventricular arrhythmias (VAs) and sudden cardiac death have become a concern in patients receiving this treatment. Older patients may be at a higher risk for developing VAs.

TRANSLATIONAL OUTLOOK: Our study suggests that patients at an advanced age should be monitored closely for VAs when treated with ibrutinib. Our findings also call for further mechanistic and clinical investigations to study how ibrutinib impacts ventricular electrophysiology. The impact of ibrutinib on electrocardiogram parameters for dispersion of repolarization, including QT dispersion and T-peak to T-end interval, may be useful features in patients' electrocardiograms indicative of ibrutinib cardiotoxicity and, hence, deserve additional study. Further work is needed to define the role of AMPK in ibrutinib-induced VAs.

REFERENCES

- Aw A, Brown JR. Current status of Bruton's tyrosine kinase inhibitor development and use in B-cell malignancies. *Drugs Aging* 2017;34:509-27.
- Burger JA, Tedeschi A, Barr PM, et al. Ibrutinib as initial therapy for patients with chronic lymphocytic leukemia. *N Engl J Med* 2015;373:2425-37.
- Wang ML, Blum KA, Martin P, et al. Long-term follow-up of MCL patients treated with single-agent ibrutinib: updated safety and efficacy results. *Blood* 2015;126:739-45.
- Wiczor TE, Levine LB, Brumbaugh J, et al. Cumulative incidence, risk factors, and management of atrial fibrillation in patients receiving ibrutinib. *Blood Adv* 2017;1:1739-48.
- Tomcsanyi J, Nenyei Z, Matrai Z, Bozsik B. Ibrutinib, an approved tyrosine kinase inhibitor as a potential cause of recurrent polymorphic ventricular tachycardia. *J Am Coll Cardiol EP* 2016;2:847-9.
- Salem JE, Manouchehri A, Bretagne M, et al. Cardiovascular toxicities associated with Ibrutinib. *J Am Coll Cardiol* 2019;74:1667-78.
- Guha A, Derbala MH, Zhao Q, et al. Ventricular arrhythmias following Ibrutinib initiation for lymphoid malignancies. *J Am Coll Cardiol* 2018;72:697-8.
- Lampson BL, Yu L, Glynn RJ, et al. Ventricular arrhythmias and sudden death in patients taking ibrutinib. *Blood* 2017;129:2581-4.
- Tuomi JM, Xenocostas A, Jones DL. Increased susceptibility for atrial and ventricular cardiac arrhythmias in mice treated with a single high dose of Ibrutinib. *Can J Cardiol* 2018;34:337-41.
- Yang T, Moslehi JJ, Roden DM. Proarrhythmic effects of Ibrutinib, a clinically approved inhibitor of Bruton's tyrosine kinase (BTK) used in cancer therapy (abstr). *Circulation* 2015;132:A14587.
- Lourey D, Sukbuntherng J, Clow F, James DF, Kunkel LA. Open label evaluation of ECG in

- patients with chronic lymphocytic leukemia (CLL) receiving ibrutinib monotherapy. *J Clin Oncol* 2013;31:7057.
12. Shanafelt TD, Parikh SA, Noseworthy PA, et al. Atrial fibrillation in patients with chronic lymphocytic leukemia (CLL). *Leuk Lymphoma* 2017;58:1630-9.
13. McMullen JR, Boey EJ, Ooi JY, Seymour JF, Keating MJ, Tam CS. Ibrutinib increases the risk of atrial fibrillation, potentially through inhibition of cardiac PI3K-Akt signaling. *Blood* 2014;124:3829-30.
14. Azam MA, Zamiri N, Masse S, et al. Effects of late sodium current blockade on ventricular re-fibrillation in a rabbit model. *Circ Arrhythm Electrophysiol* 2017;10:e004331.
15. Si D, Azam MA, Lai PFH, et al. Essential role of ryanodine receptor 2 phosphorylation in the effect of azamolene on ventricular arrhythmia vulnerability in a rabbit heart model. *J Cardiovasc Electrophysiol* 2018;29:1707-15.
16. Walker ML, Rosenbaum DS. Repolarization alternans: implications for the mechanism and prevention of sudden cardiac death. *Cardiovasc Res* 2003;57:599-614.
17. Estes NA 3rd, Michaud G, Zipes DP, et al. Electrical alternans during rest and exercise as predictors of vulnerability to ventricular arrhythmias. *Am J Cardiol* 1997;80:1314-8.
18. Momiya Y, Hartikainen J, Nagayoshi H, et al. Exercise-induced T-wave alternans as a marker of high risk in patients with hypertrophic cardiomyopathy. *Jpn Circ J* 1997;61:650-6.
19. Tse G, Wong ST, Tse V, Lee YT, Lin HY, Yeo JM. Cardiac dynamics: alternans and arrhythmogenesis. *J Arrhythm* 2016;32:411-7.
20. Hsieh YC, Lin SF, Lin TC, Ting CT, Wu TJ. Therapeutic hypothermia (30 degrees C) enhances arrhythmogenic substrates, including spatially discordant alternans, and facilitates pacing-induced ventricular fibrillation in isolated rabbit hearts. *Circ J* 2009;73:2214-22.
21. Qu Z, Garfinkel A, Chen PS, Weiss JN. Mechanisms of discordant alternans and induction of reentry in simulated cardiac tissue. *Circulation* 2000;102:1664-70.
22. Jaimes R 3rd, Walton RD, Pasdois P, Bernus O, Efimov IR, Kay MW. A technical review of optical mapping of intracellular calcium within myocardial tissue. *Am J Physiol Heart Circ Physiol* 2016;310:H1388-401.
23. Lang D, Holzem K, Kang C, et al. Arrhythmogenic remodeling of beta2 versus beta1 adrenergic signaling in the human failing heart. *Circ Arrhythm Electrophysiol* 2015;8:409-19.
24. Varro A, Negretti N, Hester SB, et al. An estimate of the calcium content of the sarcoplasmic reticulum in rat ventricular myocytes. *Pflügers Archiv* 1993;423:158-60.
25. Jiang L, Li L, Ruan Y, et al. Ibrutinib promotes atrial fibrillation by inducing structural remodeling and calcium dysregulation in the atrium. *Heart Rhythm* 2019;16:1374-82.
26. Katra RP, Laurita KR. Cellular mechanism of calcium-mediated triggered activity in the heart. *Circ Res* 2005;96:535-42.
27. Blatter LA, Kocksämper J, Sheehan KA, Zima AV, Hüser J, Lipsius SL. Local calcium gradients during excitation-contraction coupling and alternans in atrial myocytes. *J Physiol* 2003;546:19-31.
28. Weiss JN, Nivala M, Garfinkel A, Qu Z. Alternans and arrhythmias: from cell to heart. *Circ Res* 2011;108:98-112.
29. Pruvot EJ, Katra RP, Rosenbaum DS, Laurita KR. Role of calcium cycling versus restitution in the mechanism of repolarization alternans. *Circ Res* 2004;94:1083-90.
30. Mackiewicz U, Gerges JY, Chu S, et al. Ivabradine protects against ventricular arrhythmias in acute myocardial infarction in the rat. *J Cell Physiol* 2014;229:813-23.
31. Belevych AE, Terentyev D, Viatchenko-Karpinski S, et al. Redox modification of ryanodine receptors underlies calcium alternans in a canine model of sudden cardiac death. *Cardiovasc Res* 2009;84:387-95.
32. Gonzalez DR, Beigi F, Treuer AV, Hare JM. Deficient ryanodine receptor S-nitrosylation increases sarcoplasmic reticulum calcium leak and arrhythmogenesis in cardiomyocytes. *Proc Natl Acad Sci U S A* 2007;104:20612-7.
33. Oda T, Yang Y, Uchinoumi H, et al. Oxidation of ryanodine receptor (RyR) and calmodulin enhance Ca release and pathologically alter, RyR structure and calmodulin affinity. *J Mol Cell Cardiol* 2015; 85:240-8.
34. Sharif-Askari B, Doyon D, Paliouras M, Aloyz R. Bruton's tyrosine kinase is at the crossroads of metabolic adaptation in primary malignant human lymphocytes. *Sci Rep* 2019;9:11069.
35. Kocksämper J, Zima AV, Blatter LA. Modulation of sarcoplasmic reticulum Ca²⁺ release by glycolysis in cat atrial myocytes. *J Physiol* 2005; 564:697-714.
36. Kermode H, Chan WM, Williams AJ, Sitsapesan R. Glycolytic pathway intermediates activate cardiac ryanodine receptors. *FEBS Lett* 1998;431:59-62.
37. Burgoyne JR, Mongue-Din H, Eaton P, Shah AM. Redox signaling in cardiac physiology and pathology. *Circ Res* 2012;111:1091-106.
38. Han F, Li CF, Cai Z, et al. The critical role of AMPK in driving Akt activation under stress, tumorigenesis and drug resistance. *Nat Commun* 2018;9:4728.
39. Chakraborty P, Nattel S, Nanthakumar K. Linking cellular energy state to atrial fibrillation pathogenesis: potential role of adenosine monophosphate-activated protein kinase. *Heart Rhythm* 2020;17:1398-404.
40. Miyamoto T, Rho E, Sample V, et al. Compartmentalized AMPK signaling illuminated by genetically encoded molecular sensors and actuators. *Cell Rep* 2015;11:657-70.
41. Aoki K. Experimental studies on the relationship between endocrine organs and hypertension in spontaneously hypertensive rats. II. Effects of various hormones on blood pressure. *Jpn heart J* 1963;4:561-76.
42. Martínez LA, Cifuentes F, Morales MA. Ganglionic long-term potentiation in pre-hypertensive and hypertensive stages of spontaneously hypertensive rats depends on GABA modulation. *Neural Plast* 2019;2019: 7437894.

KEY WORDS action potential duration alternans, calcium handling, ibrutinib, spatial discordant repolarization, ventricular arrhythmias

APPENDIX For supplemental figures, please see the online version of this article.